Thin Solid Films 613 (2016) 68–74

Contents lists available at ScienceDirect

Thin Solid Films

journal homepage: www.elsevier.com/locate/tsf

Structural and optical studies of strain relaxation in $Ge_{1-x}Sn_x$ layers grown on Ge/Si(001) by molecular beam epitaxy

A.S. Nikolenko [a,*], V.V. Strelchuk [a], N.V. Safriuk [a], S.B. Kryvyi [a], V.P. Kladko [a], O.S. Oberemok [a], L.V. Borkovska [a], Yu.G. Sadofyev [b]

[a] V. Lashkaryov Institute of Semiconductor Physics National Academy of Sciences of Ukraine, 41 Nauky pr., 03028 Kyiv, Ukraine
[b] P.N. Lebedev Physical Institute of the Russian Academy of Sciences, 53 Leninskiy Prospekt, 119991 Moscow, Russia

ARTICLE INFO

Article history:
Received 6 July 2015
Received in revised form 19 October 2015
Accepted 27 October 2015
Available online 28 October 2015

Keywords:
Germanium-tin
Molecular beam epitaxy
High-resolution X-ray diffraction
Raman scattering
Strain relaxation

ABSTRACT

The structural and optical properties of the $Ge_{1-x}Sn_x$ layers with Sn mole fraction x of about 0.04 and 0.07 grown by molecular beam epitaxy on strain relaxed (001) Ge buffer layers have been investigated. The formation of GeSn solid solutions is proved by the high-resolution X-ray diffraction and micro-Raman investigations. The $Ge_{1-x}Sn_x$ layers are found to be partially relaxed, the degree of strain relaxation increases from 8% in the layer with $x = 0.04$ to about 14% in the layer with $x = 0.07$. For the Ge and $Ge_{1-x}Sn_x$ layers the miscut and tilt angles were calculated and compared with those predicted by Nagai's theory. For the $Ge_{1-x}Sn_x$ layer with $x = 0.07$ an abnormally large tilt of about 0.26° of the epilayer (001) lattice planes with respect to the corresponding substrate planes is found. It is shown also that the epilayer tilt axis is rotated on about 90° with respect to the direction of a substrate miscut. The possible mechanisms of the effect are discussed.

1. Introduction

The interest in the research and development of Sn-containing semiconductors based on group IV elements, in particular of GeSn alloys, is motivated by promising prospects for their usage in optoelectronic and microelectronic devices on Si platform [1]. Nowadays, Ge plays an important role in advanced optoelectronics because of its high carrier mobility and optical absorption at telecommunication wavelengths, as well as of its compatibility with existing Si processing and lattice matching with III-V semiconductors of different band gaps [2]. However, Ge is an indirect band gap semiconductor that prevents its application in light-emitting devices. The incorporation of Sn in Ge matrix offers exciting possibilities for engineering of band structure and carrier mobility in the GeSn alloy system [1].

Firstly, the systematic increase of Sn content in the GeSn alloy reduces the Γ-L valley separation and lowers the direct band gap. Theoretical calculations predict for GeSn the transition from an indirect to a direct semiconductor at around a 6–10% of Sn content in the unstrained material [3,4]. The room-temperature photoluminescence originated from direct band gap transitions in the GeSn layers [5,6] as well as the electroluminescence from diode structures with active GeSn layers [7–10] have been observed.

The reduction of the energy gap in the GeSn alloy leads also to a substantial improvement in the absorption properties in the infrared wavelength range up to 1800 nm. It has been shown that Sn concentrations as small as 2% are sufficient to achieve absorption coefficients that cover the whole telecommunication windows and are at least 10-fold higher as compared with Ge in C- and L-bands [11]. The GeSn p–i–n photodetectors fabricated by standard processes fully compatible with conventional Si complementary metal-oxide semiconductor technology are found to be highly attractive for applications in both optical communications and optical interconnects [12–14].

GeSn alloys are predicted also to have an increased electron and hole mobility by a factor of 4 as compared with Ge [15] which makes it promising to use as a channel material in metal oxide semiconductor field effect transistors (MOSFETs). In fact, GeSn pMOSFETs with channel Sn composition of 7% showed enhancement in hole mobility over control Ge devices by 85% [16].

The unstrained buffer layers of GeSn can be used also as uniaxial compressive stressors for Ge channels in high performance Ge-MOSFETs and tunnel-field effect transistors [17,18] owing to larger lattice parameter of GeSn as compared with Ge. The advantages of uniaxially strained Ge channels are: higher drift current, high hole mobility and smaller shift of threshold voltage compared to the biaxially strained ones.

Thereby, both fully strained and strain relaxed GeSn layers of different Sn content are of interest for application in modern optoelectronic and microelectronic devices. However, epitaxial growth of GeSn alloys faces the challenges of large lattice mismatch between Ge and α-Sn (~14.7%), low solubility of Sn in the Ge matrix (~1%) and Sn surface segregation at growth temperatures higher than 140 °C [19]. To inhibit Sn

* Corresponding author.
E-mail address: nikolenko_mail@ukr.net (A.S. Nikolenko).

http://dx.doi.org/10.1016/j.tsf.2015.10.065
0040-6090/

segregation in GeSn alloy the low growth temperatures are required though the low temperature growth results in the surface roughening and limited critical epitaxial thicknesses [20]. It has been demonstrated that metastable GeSn films with Sn content up to 26% and no signs of Sn segregation can be grown epitaxially on Ge substrate at temperatures lower than 100 °C [20]. The understanding of the mechanisms of strain relaxation in the GeSn/Ge heterostructures is of particular importance for their advantageous use in modern devices.

This study presents the results of structural and optical investigations of $Ge_{1-x}Sn_x$ films with x of about 0.04 and 0.07 grown on relaxed Ge layers by molecular beam epitaxy (MBE).

2. Experimental details

The Ge and GeSn layers were grown by MBE in a Katun MBE system. Growth mode was controlled in situ by reflection high energy electron diffraction (RHEED).

Ge buffer layers of 1.5 μm thickness were grown on (001) Si substrates at a temperature of 650 °C. A two domain reconstruction of type $(2 \times 1) + (1 \times 2)$, which is typical for the (001) orientation, was observed in the RHEED patterns for the surface of the Ge buffer layers.

The GeSn layers of about 0.4 μm thickness and Sn content of about 4% or 7% were grown on Ge buffer layers at a temperature of 150 °C and a deposition rate of 8 nm/min. The observed RHEED patterns indicate that the epitaxy of the GeSn layers proceeds with the same type of surface reconstruction as the Ge buffer layers at 650 °C, but is accompanied with the formation of facets on the surface of GeSn layer. The surface roughness of the films was studied by atomic force microscopy. A root-mean-square roughness was found to be about 1 nm for the Ge buffer layer and in the range of 4–6 nm for the GeSn layers.

Three types of heterostructures were investigated: (i) 1.5 μm Ge buffer layer grown on Si substrate; (ii) 0.4 μm $Ge_{0.96}Sn_{0.04}$ layer grown on 1.5 μm Ge buffer layer/Si substrate; and (iii) 0.4 μm $Ge_{0.93}Sn_{0.07}$ layer grown on 1.5 μm Ge buffer layer/Si substrate.

The structural properties of the samples were studied by the high-resolution X-ray diffraction (HRXRD) and secondary neutral mass spectrometry (SNMS) methods. The HRXRD measurements were carried out using a high resolution X-ray diffractometer X'Pert PRO MRD with a 4 × Ge (220) monochromator and Cu anode. The SNMS measurements were performed in the high frequency (HF) mode of the sample sputtering by Ar^+ ions with energy 300 eV in INA-3 (Laybold-Heraeus, Germany) instrument. These ions were generated due to the application of HF voltage in the form of rectangular negative pulses between sample and wall of the low pressure (3.26×10^{-2} mbar) argon radiofrequency (27.12 MHz) plasma. The voltage frequency was 100 kHz (50% duty cycle). The area of sputtering was limited by the tantalum diaphragm with the internal diameter 3 mm. The sputtering rate was approximately 0.5 nm/s. The depth scale was determined for each profile by measuring the crater depth with a Dektak 3030 profilometer.

The micro-Raman study was done using a triple Raman spectrometer T-64,000 Horiba Jobin-Yvon with an excitation by a 647.0 nm line of an Ar–Kr ion laser at room temperature in the backscattering from (100) plane in parallel $z(x,x)\bar{z}$and crossed $z(x,y)\bar{z}$-geometries, where x, y and z correspond to {100}, {010} and {001} directions of the cubic crystal structure, correspondingly.

3. Results and discussion

3.1. SNMS investigations

Fig. 1 shows the SNMS profiles for Sn and Ge distribution in the depth of GeSn films. The SNMS investigations reveal the Sn content in the ranges of 3.5–4% and 7.5–8.3% for two GeSn films studied. The distribution of Sn is found to be rather uniform excepting for a lower Sn content at the beginning of the growth, i.e. in the first 30–50 nm of the GeSn films. A formation of compositionally graded layer with reduced Sn content near the GeSn/Ge interface has been reported for the GeSn films grown on Ge by MBE [21] or chemical vapor deposition (CVD) [22]. This was explained by the growth mechanism including rate-limiting incorporation of Sn from a surface adlayer [21].

In fact, the Sn depth profile in the GeSn layer with 7% of Sn shows an increased Sn content (up to about 16%) near the film surface. A thickness of this Sn-enriched region is of about 1.5–2 nm that is smaller than depth resolution of the SNMS method of ~4 nm. Therefore, we cannot distinguish between thin Sn-rich near surface region caused by Sn precipitation and the increased Sn signal caused by the presence of residual impurities, oxide or other contaminations on the film surface. As a rule, Sn precipitation occurs during the growth or upon the post-deposition thermal treatment in the two ways: (i) formation of Sn-rich nanoparticles at around the surface of the film or within the layer, and (ii) formation of thin Sn-enriched layer near the film surface. The reported sizes of Sn inhomogeneities vary from tens to several hundred nanometers [20,23–25]. The SNMS investigations do not reveal large depth inhomogeneities of Sn distribution in the GeSn films studied. However, it cannot exclude the presence of small Sn-rich precipitates owing to low spatial resolution in lateral direction of the SNMS method.

3.2. Raman spectra investigations

The Raman spectra of the structures studied (Fig. 2) show a strong Ge LO phonon peak in the range of 297–302 cm^{-1}. Besides the Ge–Ge phonon mode, the Raman spectra of the GeSn films exhibit a clear Sn–Sn vibration mode in the range of 180–186 cm^{-1} and a Ge–Sn mode in the range of 259–264 cm^{-1}. These modes are not observed in pure Ge buffer layer and are the evidence of GeSn solid solution formation.

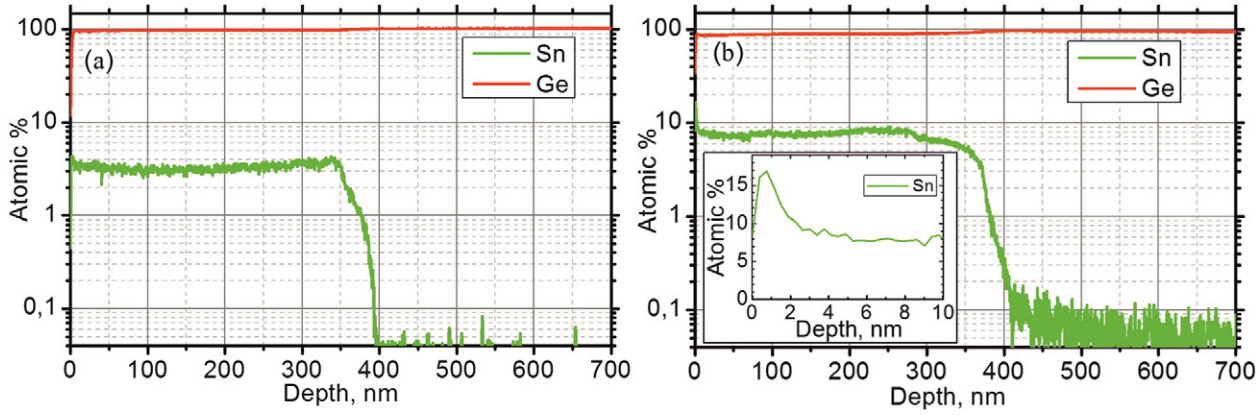

Fig. 1. SNMS depth profiles of Sn and Ge distribution in the structures with Sn content of about 4% (a) and 7% (b).

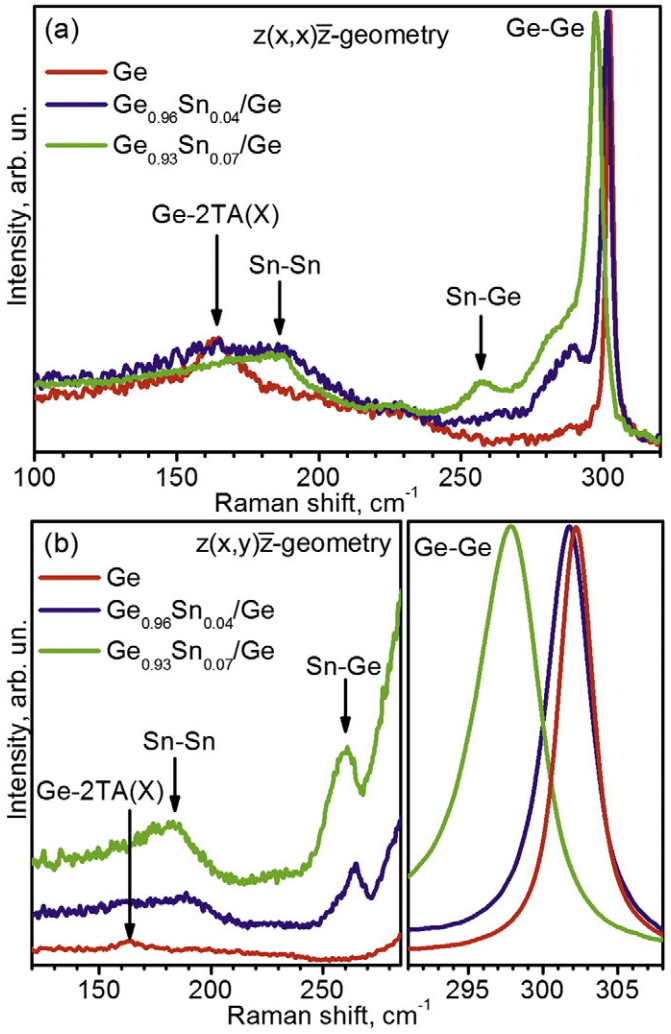

Fig. 2. Raman spectra of the investigated structures measured in parallel (a) and crossed (b) polarizations in $z(x,x)\bar{z}$and $z(x,y)\bar{z}$-scattering geometries, correspondingly.

Measurement in crossed polarization of the exciting and scattered radiation ($z(x,y)\bar{z}$-geometry) make it possible to decrease the contribution of two-phonon 2TA(X) scattering and to make Sn–Sn phonon band more pronounced (Fig. 2b). The frequencies and full width at a half maximum (FWHM) of three experimentally observed phonon modes are listed in Table 1.

All three Raman modes shift to lower wave numbers as the Sn content in the GeSn alloy increases (Table 1). Since the Raman frequency shift in semiconductor alloys is influenced mainly by composition and strain, the change in the Ge–Ge phonon mode frequency can be presented as the sum of the changes caused by formation of solid solution (composition term) and induced by elastic deformations (strain term):

$$\Delta\omega_{\text{Ge–Ge}} = \Delta\omega_{\text{alloy}} + \Delta\omega_{\text{strain}} \ .$$

Table 1
Experimental phonon frequencies and the FWHM of the phonon modes.

The film/phonon mode	Sn–Sn		Sn–Ge		Ge–Ge	
	ω, cm^{-1}	Γ, cm^{-1}	ω, cm^{-1}	Γ, cm^{-1}	ω, cm^{-1}	Γ, cm^{-1}
Ge	–	–	–	–	302.2	2.8
GeSn/Ge (Sn = 4%)	186.6	43.7	264.4	12.8	301.8	3.5
GeSn/Ge (Sn = 7%)	180.2	52.1	259.7	23.2	297.8	5.0

For completely relaxed $Ge_{1-x}Sn_x$ alloys, the composition term is theoretically predicted [26] to vary with Sn content as $\Delta\omega_{\text{alloy}} = -95.1\times$. For fully strained $Ge_{1-x}Sn_x$ layers on Ge (001), theoretical analysis predicts the dependencies for the strain term: $\Delta\omega_{\text{strain}} = 64.0\times$ and for the change in the Raman frequency of the Ge–Ge mode: $\Delta\omega_{\text{Ge-Ge}} = -31.1\times$ [26].

A comparison of the experimentally observed frequencies of the Ge–Ge mode in the two studied $Ge_{1-x}Sn_x$ layers with theoretically predicted ones for both fully strained and completely relaxed layers shows that the layer with Sn content of about 4% is fully strained, while the layer with 7% of Sn is partially relaxed.

The incorporation of Sn produces not only the shift of the Raman phonon modes, but also the increase of their FWHM (Table 1). The latter testifies to general deterioration of the crystal quality of the GeSn alloy.

3.3. XRD study

The high resolution symmetric reciprocal space maps (RSMs) near the (004) Bragg peaks and the asymmetric RSMs for the (113) Bragg reflections of the structures studied are presented in Figs. 3 and 4, respectively. In the RSMs of the Ge/Si structure, two intense features attributed to the reciprocal lattice peaks from the Si substrate and Ge buffer layer are found (Figs. 3a and 4a). An appearance of GeSn peak in the XRD maps of the GeSn/Ge structures testifies to the formation of GeSn solid solution. The GeSn diffraction peak in the symmetric RSM (Fig. 3) shows relatively narrow intensity distribution for the layer with 4% of Sn ($\Delta Q_x = 0.00307$, $\Delta Q_y = 0.0033$) and much broader for the GeSn layer with 7% of Sn ($\Delta Q_x = 0.0053$, $\Delta Q_y = 0.0082$). This indicates deterioration in the quality of the GeSn layer as the Sn concentration increases.

In the symmetric (004) RSMs, the nearly ideal vertical alignment of the Si and Ge peaks, as well as a peak from the GeSn layer with 4% of Sn is observed which means that the (001) crystallographic planes in these layers and in the Si substrate are parallel. At the same time, the peak from the GeSn layer with 7% of Sn is found to be shifted along the Q_x axis with regard to the peak of Ge, which implies the misorientation between the (001) planes in the Ge and $Ge_{0.93}Sn_{0.07}$ layers. This phenomenon is even better shown in two asymmetric (113) RSMs of this heterostructure recorded when turning the sample at a 180° (Fig. 4c, d). In these two maps, the peak from the $Ge_{0.93}Sn_{0.07}$ layer is found to be shifted in opposite directions along the Qx axis relative to the Ge peak as a result of tilting of the (001) planes of the $Ge_{0.93}Sn_{0.07}$ layer.

The tilting of the epilayer lattice planes with respect to the corresponding substrate planes is usually encountered in the lattice mismatched heterostructures when a miscut (vicinal) substrate is used [27]. To evaluate a possible miscut of the Si substrates as well as a tilt for both the Ge and GeSn epilayers, the (004) rocking curves were recorded for different azimuthal angles in 10° increments. The variation of Si, Ge and GeSn peak positions with azimuthal angle of the incoming X-rays (Fig. 5) shows the sinusoidal dependence in all structures studied. For a Si peak, the sinusoidal dependence is caused entirely by the misorientation of the substrate (001) axis from a surface normal. The miscut angle for a Si substrate estimated as amplitude of a sinusoidal curve varies from 0.18 to 0.4° in different samples (Table 2). The azimuthal dependence for the Ge and $Ge_{0.96}Sn_{0.04}$ peak positions follows those for the Si substrate peak in the corresponding structure. The amplitudes of these sinusoidal dependencies are shown in Table 2 and referred to miscut angles. The difference in the miscut angles for the Ge or $Ge_{0.96}Sn_{0.04}$ layers and the miscut of Si substrate determines a relative tilt of the (001) lattice planes of corresponding epilayer and an underlying layer. The estimated tilt for the Ge and $Ge_{0.96}Sn_{0.04}$ layers (Table 2) varies in the range 0.002–0.009° and is negligibly small which indicates that the (001) planes in these layers and in the Si substrate are nearly parallel.

At the same time, the sinusoidal dependence for the $Ge_{0.93}Sn_{0.07}$ peak position is found to be shifted on about 90° relative to those for

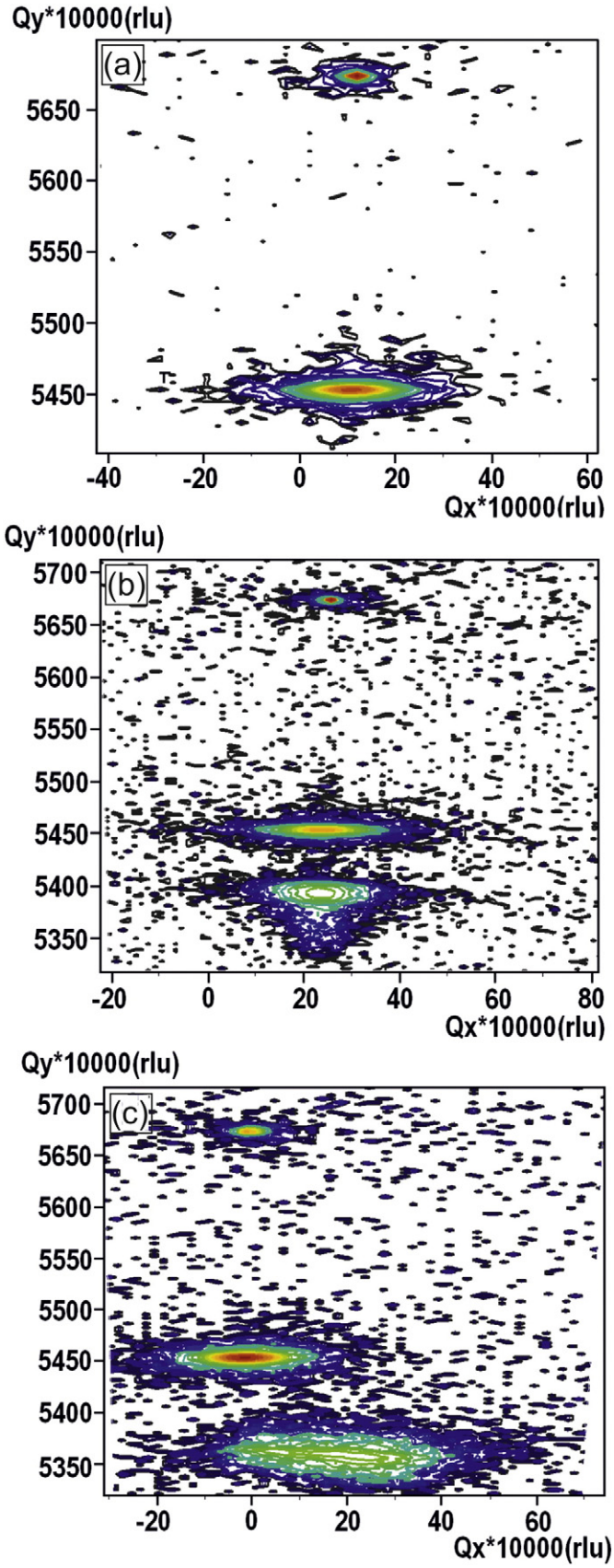

Fig. 3. Symmetric RSM from (004) reflection of Ge buffer layer on Si (a), $Ge_{0.96}Sn_{0.04}$ layer grown on Ge buffer layer (b) and $Ge_{0.93}Sn_{0.07}$ layer grown on Ge buffer layer (c).

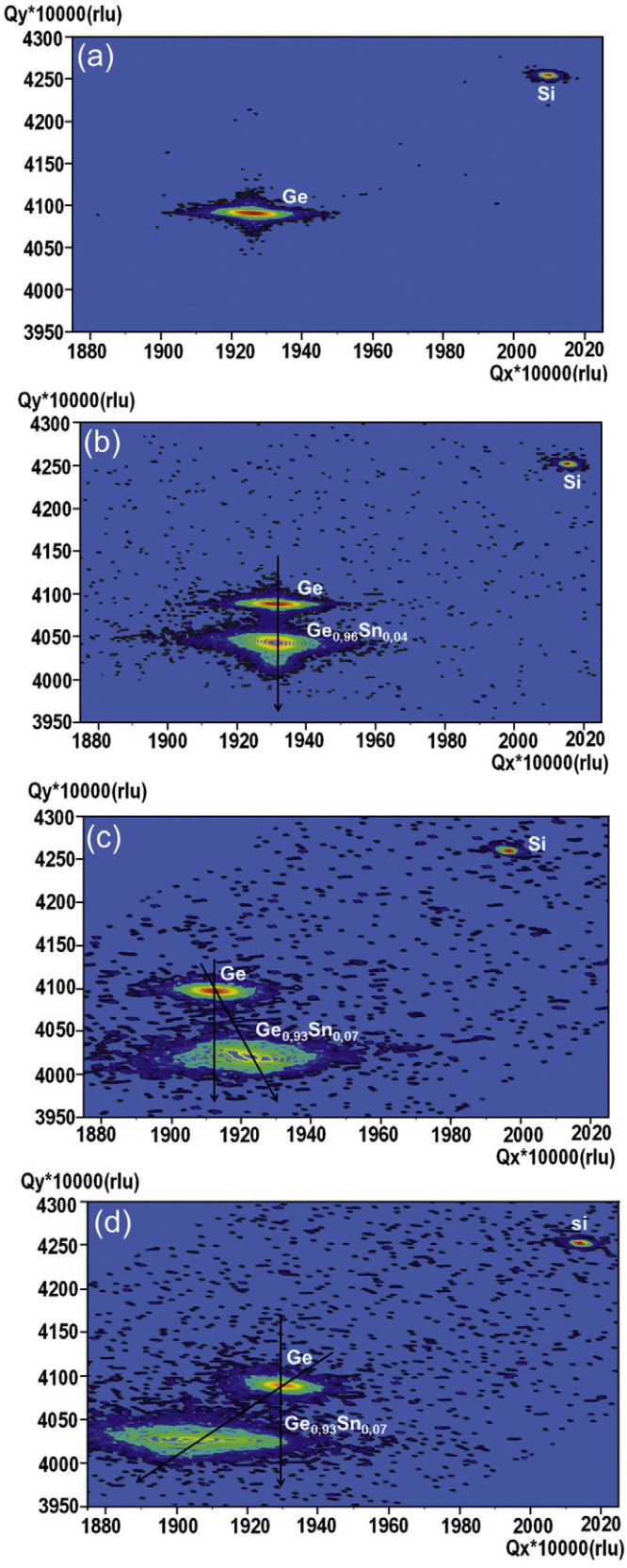

Fig. 4. Asymmetric RSM from (113) reflection of Ge buffer layer on Si (a), $Ge_{0.96}Sn_{0.04}$ layer on Ge buffer layer (b), $Ge_{0.93}Sn_{0.07}$ layer on Ge buffer layer at $\varphi = 0°$ (c) and $\varphi = 180°$ (d).

the Si and Ge peaks (Fig. 5c). Although the miscut angle for the $Ge_{0.93}Sn_{0.07}$ layer (~0.162°) is close to the values obtained for the Si substrate (~0.195°) and Ge (~0.201°) layer, the rotation of the tilt axis

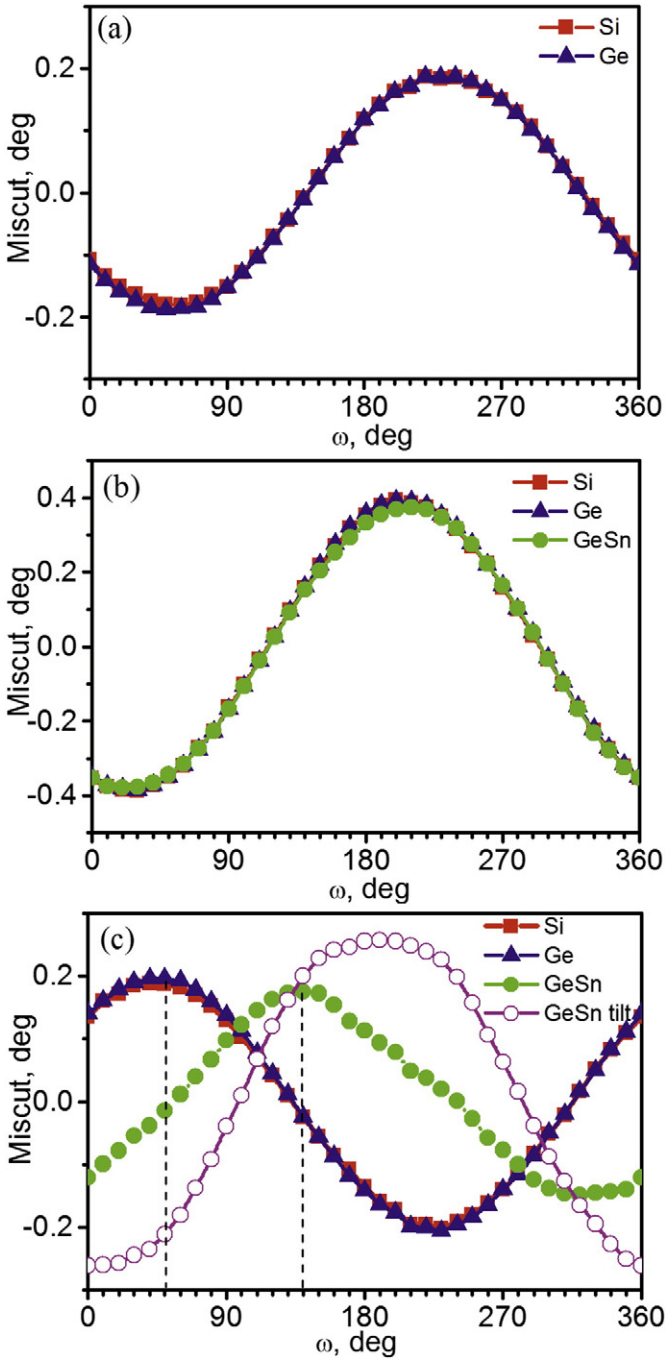

Fig. 5. Miscut angle for the Si substrate (squares), Ge buffer layer (triangles), GeSn layer (circles) and tilt angle for GeSn layer (open circles) for the Ge/Si (a), $Ge_{0.96}Sn_{0.04}$/Ge/Si (b) ad $Ge_{0.93}Sn_{0.07}$/Ge/Si (c) heterostructures.

produces noticeable tilt of about 0.2° of the (001) planes of $Ge_{0.93}Sn_{0.07}$ epilayer with respect to the (001) planes of the underlying Ge buffer layer (Fig. 5).

Both the miscut and rotating tilting can complicate estimation of the lattice constants for the epilayers studied. To minimize this effect, both the symmetric (004) and asymmetric (113) RSMs were used for calculation of the lattice parameters. From the symmetric (004) RSMs the lattice constant in the direction perpendicular to the interface plane, $a^{\perp}$, can be calculated using the ratios:

$$a^{\perp}=4\cdot d_{004},$$
$$d_{004}=1/Q,$$
$$Q^2=Q_x{}^2+Q_y{}^2,$$

where d_{004} is the interplanar spacing for (004) plane, Q is the reciprocal lattice vector, Q_y and Q_x are the reciprocal space coordinates perpendicular and parallel to the surface, respectively.

The lattice constant in the direction parallel to the interface plane, $a^{\parallel}$, can be calculated using the estimated values of $a^{\perp}$ and the relation for the interplanar spacings d^2_{hkl} for a family of planes with Miller indices (hkl) for a tetragonal lattice:

$$d^2{}_{hkl}=\left[h^2+k^2+l^2\left(a^{\parallel}/a^{\perp}\right)^2\right]/a^{\parallel 2},$$

where the d_{113} is obtained from the asymmetric (113) RSMs. The calculated lattice parameters, $a^{\perp}$ and $a^{\parallel}$, for the structures studied as well as the bulk lattice constants for Si, Ge and GeSn are summarized in Table 2. The lattice parameters for the GeSn layers a_{GeSn} for certain Sn content x are calculated using the Vegard's law:

$$a_{GeSn}=(1-x)\cdot a_{Ge}+x\cdot a_{Sn},$$

where a_{Ge} is the lattice constant of bulk Ge, a_{Sn} = 6.489 A is the lattice constant of cubic α-Sn.

The calculated in-plane lattice constants are found to be smaller than the bulk values. This means that both the Ge and GeSn layers remain under biaxial compressive strains which are small in Ge buffer layer ($\sim 1\cdot 10^{-3}$) and increase distinctly in the GeSn layers ($\sim 6.7\cdot 10^{-3}$ for the $Ge_{0.96}Sn_{0.04}$ layer and $\sim 1.0\cdot 10^{-2}$ for the $Ge_{0.93}Sn_{0.07}$ layer). At the same time, the calculated vertical lattice parameters for the GeSn layers are found to be larger than the bulk values indicating tetragonal distortion of the crystal lattice.

The degree of strain relaxation in the GeSn layers, R_{GeSn}, was calculated using the estimated in-plane lattice constants for the GeSn ($a^{\parallel}{}_{GeSn}$) and Ge ($a^{\parallel}{}_{Ge}$) layers, from the ratio:

$$R_{GeSn}=\left(a^{\parallel}{}_{GeSn}-a^{\parallel}{}_{Ge}\right)/\left(a_{GeSn}-a^{\parallel}{}_{Ge}\right).$$

The similar procedure was done for the Ge layers and the results are listed in Table 2. The Ge buffer layers are found to be almost completely relaxed, while the GeSn layers are only partially relaxed. The degree of strain relaxation in the GeSn layer increases from 8% in the layer with

Table 2
The experimentally obtained miscut and tilt angles, the tilt angles estimated from Nagai theory, estimated values of the lattice constants in the directions perpendicular and parallel to the interface, bulk lattice constants and degree of strain relaxation for the layers in the structures studied.

The structure studied	Layer studied	Miscut, degree	Tilt (experiment), degree	Tilt (Nagai), degree	$a^{\perp}$, Å	$a^{\parallel}$, Å	a, Å	R, %
Ge/Si	Si	0.1833	–	–	5.43044	5.430119	5.431	–
	Ge	0.1876	0.0043	0.0073	5.650324	5.646802	5.658	95%
GeSn/Ge (Sn = 4%)	Si	0.4036	–	–	5.43038	5.427551	5.431	–
	Ge	0.4055	0.0019	0.0164	5.650508	5.649518	5.658	96%
	GeSn	0.397	−0.0084	0.0045	5.713216	5.65289	5.69124	8%
GeSn/Ge (Sn = 7%)	Si	0.1951	–	–	5.430793	5.426115	5.431	–
	Ge	0.2014	0.0063	0.0079	5.649892	5.648824	5.658	97%
	GeSn	0.1622	−0.2109	0.00354	5.751836	5.658298	5.71617	14%

4% of Sn to about 14% in the layer with 7% of Sn. The increase of strain relaxation agrees with larger FWHM of the GeSn diffraction peak for the GeSn layer with 7% of Sn.

The GeSn layers are also characterized by a tilt of the epilayer lattice planes with respect to the corresponding substrate planes. As a rule, two origins of the tilt in lattice mismatched heterostructures are considered: (i) the elastic strain exerted by the substrate surface steps, and (ii) the contribution from misfit dislocations with Burgers vectors inclined to growth surface [28]. The tilt of the first type, the so called Nagai tilt, is a simple geometrical consequence of lattice misfit and substrate surface steps [29]. The model implies two-dimensional growth of the layer which starts at the substrate steps. The epilayer is considered to be tetragonally distorted, the lattice constant of epilayer is supposed to change from a^s (the lattice constant of a substrate) to $a^{\perp}$ (the epilayer lattice constant in the growth direction) over the length of a substrate step. This produces a tilt, $\Delta\alpha$, of the epilayer which can be calculated from the equation:

$$\tan\Delta\alpha = \left(a^{\perp} - a^{s}\right)/a^{s} \cdot \tan\varphi,$$

where φ is the substrate miscut angle. The calculated Nagai's tilts for both the Ge and GeSn layers listed in Table 2 agree passably with the tilt values estimated from the XRD maps except for the GeSn layer with 7% of Sn. In the latter case the relative tilt of the epilayer and the substrate planes (~0.21°) is much larger than those predicted by Nagai's model (~0.00354°).

The Nagai's model [29] predicts also that the direction of tilt will be away from the offcut direction in the case of $a^{\perp} > a^{s}$ (positive tilt) and toward the offcut direction for $a^{\perp} < a^{s}$ (negative tilt). In all structures studied, the positive tilt should be observed for both the Ge and GeSn layers in accordance with the Nagai's model. However, a tilt for the GeSn layers is found to be negative, while those for the Ge layers are positive. Therefore, it can be supposed that a tilting of GeSn lattice plains is governed by the second mechanism mention above, i.e. by generation of misfit dislocations.

The tilt of (001) diamond or zincblende lattice is often ascribed to the unequal formation of 60° misfit dislocations lying along the two [110] directions at the interface [28]. These dislocations have a screw component and a tilt component, as well as the misfit component which provides the driving force for their introduction. In the case of a perfectly cut substrate, the screw and tilt components play no role, because, when all possible dislocations are generated in equal numbers, the screw and tilt components cancel out, leaving only a net misfit component [30]. The effect of miscut is to decrease the activation barrier for nucleation on one slip system compared to its value in the case of a perfectly oriented substrate [30]. A preferential formation of dislocations with specific tilt component causes net tilting of the epilayer lattice planes. In the case of the tilt caused by misfit dislocation formation the tilt angle depends not only on the substrate miscut and misfit magnitude but also on the mechanism and degree of strain relaxation [30].

The rotated tilt is expected only when the miscut direction is not [110] and either the substrate or the epilayer (or both of them) is polar [31]. Therefore, rotated tilt is not expected for the Ge layers grown on Si substrate even though the substrate miscut direction is toward [100]. The rotated tilting has been observed in large-misfit systems like InP [32], ZnSe, ZnTe and CdZnTe [33] layers grown on GaAs substrate, $BiFeO_3$ layers grown on $SrTiO_3$ substrate [34], etc. Up to date, there is no general theory describing the mechanism of rotated tilt formation. For the InP/GaAs system the rotation of the tilt axis has been attributed to the temperature-dependent anisotropy of the initial 3D nucleation process which is thought to be caused by the anisotropic surface diffusion lengths of In atoms along the orthogonal [110] directions [32]. It has been found that the lower is the nucleation temperature the larger is the rotated tilt magnitude. We also observe rotated tilt in the large-misfit structure (the lattice mismatch is of about 1%) grown at low temperature. However, the RHEED patterns do not show a 3D growth mode but reveal the formation of facets. Moreover, the relaxation degree of the GeSn layer is relatively low which implies low dislocation density. In fact, the surface morphology of the $Ge_{1-x}Sn_x$ films with $x < 0.09$ growing on (001) Ge substrate at low temperatures has been shown to be controlled by kinetic surface roughening [20]. The latter is caused by the presence of Ehrlich barriers to the migration of adatoms over down-steps on growing surfaces and results in surface facetting with increasing film thickness. At higher Sn concentrations ($x > 0.09$) the surface morphology evolution is controlled by strain-induced roughening which results in coherent 3D islanding providing partial relaxation through elastic deformation and dilatation [20]. We can suppose that rotated tilt observed for GeSn layer with Sn content of about 7% results mainly from local surface tilting caused by formation of facets. The latter can be due to anisotropy of dislocation distribution in the layer.

4. Conclusions

The structural and optical properties of the $Ge_{1-x}Sn_x$ layers with $x = 0.04$ and 0.07 have been investigated using HRXRD, SNMS and Raman scattering. The GeSn layers are grown by MBE on Ge buffer layer at low temperature (~150 °C) and the Ge buffer layer is grown on (001) Si substrate at ~650 °C. The formation of GeSn solid solutions is proved by both HRXRD and Raman investigations. In particular, in the Raman spectra of the GeSn films the Sn–Sn, Sn–Ge and Ge–Ge phonon modes were observed. The positions of the observed modes reflect the changes in concentration x and strains of the $Ge_{1-x}Sn_x$ films. The SNMS studies show rather uniform distribution of Sn in the GeSn layer. From the symmetric and asymmetric HRXRD maps the lattice parameters, degree of strain relaxation, miscut and tilt of the epilayer (001) lattice planes with respect to the corresponding substrate planes were estimated. It is found that the Ge layers are almost completely relaxed, while the GeSn layers are strained (the degree of strain relaxation does not exceed 14% for $x = 0.07$). A tilt angle of the Ge and GeSn lattice planes is found to be small (<0.01°) that agrees well with those predicted by Nagai's mechanism for a substrate with small miscut (0.2–0.4°). For the $Ge_{1-x}Sn_x$ film with $x = 0.07$ a tilt of about 0.2° caused mainly by rotation of a tilt axis on about 90° with respect to the substrate miscut is revealed. The rotation of a tilt axis is supposed to be caused mainly by local surface tilting owing to the formation of facets resulted from the anisotropy of dislocation distribution in the layer.

References

[1] J. Kouvetakis, J. Menendez, A.V.G. Chizmeshya, Tin-based group IV semiconductors: new platforms for opto- and microelectronics on silicon, Annu. Rev. Mater. Res. 36 (2006) 497–554.

[2] L.C. Kimerling, Photons to the rescue: microelectronics becomes microphotonics, Electrochem. Soc. Interface 9 (2000) 28–31.

[3] V.R. D'Costa, C.S. Cook, A.G. Birdwell, C.L. Littler, M. Canonico, S. Zollner, J. Kouvetakis, J. Menendez, Optical critical points of thin-film Ge1.ySny alloys: A comparative $Ge_{1-y}Sn_y/Ge_{1-x}Si_x$ study, Phys. Rev. B 73 (125207) (2006) 1–16.

[4] W.J. Yin, X.G. Gong, S.H. Wei, Origin of the unusually large band-gap bowing and the breakdown of the band-edge distribution rule in the Sn_xGe_{1-x} alloys, Phys. Rev. B 78 (161203) (2008) 1–-4.

[5] J. Mathews, R.T. Beeler, J. Tolle, C. Xu, R. Roucka, J. Kouvetakis, J. Menendez, Direct-gap photoluminescence with tunable emission wavelength in $Ge_{1-y}Sn_y$ alloys on silicon, Appl. Phys. Lett. 97 (2010) 221912.

[6] R. Chen, H. Lin, Y. Huo, C. Hitzman, T.I. Kamins, J.S. Harris, Increased photoluminescence of strain-reduced, high-Sn composition $Ge_{1-x}Sn_x$ alloys grown by molecular beam epitaxy, Appl. Phys. Lett. 99 (2011) 181125.

[7] R. Roucka, J. Mathews, R.T. Beeler, J. Tolle, J. Kouvetakis, J. Menéndez, Direct gap electroluminescence from $Si/Ge_{1-y}Sn_y$ p–i–n heterostructure diodes, Appl. Phys. Lett. 98 (2011) 061109.

[8] H.H. Tseng, K.Y. Wu, H. Li, V. Mashanov, H.H. Cheng, G. Sun, R.A. Soref, Mid-infrared electroluminescence from a $Ge/Ge_{0.922}Sn_{0.078}/Ge$ double heterostructure p–i–n diode on a Si substrate, Appl. Phys. Lett. 102 (2013) 182106.

[9] J.P. Gupta, N. Bhargava, S. Kim, T. Adam, J. Kolodzey, Infrared electroluminescence from GeSn heterojunction diodes grown by molecular beam epitaxy, Appl. Phys. Lett. 102 (2013) 251117.

[10] M. Oehme, J. Werner, M. Gollhofer, M. Schmid, M. Kaschel, E. Kasper, J. Schulze, Room-temperature electroluminescence from GeSn light-emitting pin diodes on Si, IEEE Photon. Technol. Lett. 23 (2011) 1751–1753.
[11] V.R. D'Costa, Y. Fang, J. Mathews, R. Roucka, J. Tolle, J. Menendez, J. Kouvetakis, Sn-alloying as a means of increasing the optical absorption of Ge at the C- and L-telecommunication bands, Semicond. Sci. Technol. 24 (115006) (2009) 8.
[12] S. Su, B. Cheng, C. Xue, W. Wang, Q. Cao, H. Xue, W. Hu, G. Zhang, Y. Zuo, Q. Wang, GeSn p–i–n photodetector for all telecommunication bands detection, Opt. Express 19 (2011) 6400–6405.
[13] M. Oehme, M. Schmid, M. Kaschel, M. Gollhofer, D. Widmann, E. Kasper, J. Schulze, GeSn p–i–n detectors integrated on Si with up to 4% Sn, Appl. Phys. Lett. 101 (2012) 141110.
[14] D. Zhang, C. Xue, B. Cheng, S. Su, Z. Liu, X. Zhang, G. Zhang, C. Li, Q. Wang, High-responsivity GeSn short-wave infrared p–i–n photodetectors, Appl. Phys. Lett. 102 (2013) 141111.
[15] J.D. Sau, M.L. Cohen, Possibility of increased mobility in Ge–Sn alloy system, Phys. Rev. B 75 (045208) (2007) 1–-7.
[16] S. Gupta, Y.-C. Huang, Y. Kim, E. Sanchez, K.C. Saraswat, Hole mobility enhancement in compressively strained $Ge_{0.93}Sn_{0.07}$ pMOSFETs, IEEE Electron. Device Lett. 34 (2013) 831–833.
[17] S. Takeuchi, Y. Shimura, T. Nishimura, B. Vincent, G. Eneman, T. Clarysse, J. Demeulemeester, A. Vantomme, J. Dekoster, M. Caymax, R. Loo, A. Sakai, O. Nakatsuka, S. Zaima, $Ge_{1-x}Sn_x$ stressors for strained-Ge CMOS, Solid State Electron. 60 (2011) 53–57.
[18] A. Vincent, Y. Shimura, S. Takeuchi, T. Nishimura, G. Eneman, A. Firrincieli, J. Demeulemeester, Vantomme, T. Clarysse, O. Nakatsuka, S. Zaima, J. Dekoster, M. Caymax, R. Loo, Characterization of GeSn materials for future Ge pMOSFETs source/drain stressors, Microel. Eng. 88 (2011) 342–346.
[19] W. Wegscheider, K. Eberl, U. Menczigar, G. Abstreiter, Single crystal Sn/Ge super lattices on Ge substrates: growth and structural properties, Appl. Phys. Lett. 57 (1990) 875.
[20] O. Gurdal, P. Desjardins, J.R.A. Carlsson, N. Taylor, H.H. Radamson, J.-E. Sundgren, J.E. Greene, Low-temperature growth and critical epitaxial thicknesses of fully strained metastable $Ge_{1-x}Sn_x$ ($x \le 0.26$) alloys on Ge(001)2×1, J. Appl. Phys. 83 (1998) 162–170.
[21] P.R. Pukite, A. Harwit, S.S. Iyer, Molecular beam epitaxy of metastable, diamond structure Sn_xGe_{1-x} alloys, Appl. Phys. Lett. 54 (1989) 2142–2144.
[22] F. Gencarelli, B. Vincent, J. Demeulemeester, A. Vantomme, A. Moussa, A. Franquet, A. Kumar, H. Bender, J. Meersschaut, W. Vandervorst, R. Loo, M. Caymax, K. Temst, M. Heynsa, Crystalline properties and strain relaxation mechanism of CVD grown GeSn, ECS J. Solid State Sci. Technol. 2 (2013) P134–P137.
[23] R. Chen, Y.-C. Huang, S. Gupta, A.C. Lin, E. Sanchez, Y. Kim, K.C. Saraswat, T.I. Kamins, J.S. Harris, Material characterization of high Sn-content, compressively-strained GeSn epitaxial films after rapid thermal processing, J. Cryst. Growth 365 (2013) 29–34.
[24] H. Li, Y.X. Cui, K.Y. Wu, W.K. Tseng, H.H. Cheng, H. Chen, Strain relaxation and Sn segregation in GeSn epilayers under thermal treatment, Appl. Phys. Lett. 102 (2013) 251907.
[25] T. Tsukamoto, N. Hirose, A. Kasamatsu, T. Mimura, T. Matsui, Y. Suda, Investigation of Sn surface segregation during GeSn epitaxial growth by Auger electron spectroscopy and energy dispersive X-ray spectroscopy, Appl. Phys. Lett. 106 (2015) 052103.
[26] S. Su, W. Wang, B. Cheng, W. Hu, G. Zhang, C. Xue, Y. Zuo, Q. Wang, The contributions of composition and strain to the phonon shift in $Ge_{1-x}Sn_x$ alloys, Solid. State Commun. 151 (2011) 647–650.
[27] F. Riesz, Crystallographic tilting in latticemismatched heteroepitaxy: a Dodson–Tsao relaxation approach, J. Appl. Phys. 79 (1996) 4111–4117.
[28] J.E. Ayers, S.K. Ghandhi, L.J. Schowalter, Crystallographic tilting of heteroepitaxial layers, J. Cryst. Growth 113 (1991) 430–440.
[29] H. Nagai, Structure of vapordeposited $Ga_xIn_{1-x}As$ crystals, J. Appl. Phys. 45 (1974) 3789–3794.
[30] P. Mooney, F.K. LeGoues, J. Tersoff, J.O. Chu, Nucleation of dislocations in SiGe layers grown on (001) Si, J. Appl. Phys. 75 (1994) 3968–3977.
[31] F. Riesz, Rotated tilting in lattice-mismatched heteroepitaxial systems, J. Cryst. Growth 140 (1994) 213–218.
[32] F. Riesz, K. Lischka, K. Rakennus, T. Hakkarainen, A. Pesek, Tilting of lattice planes in InP epilayers on miscut GaAs substrates: the effect of initial growth conditions, J. Cryst. Growth 114 (1991) 127–132.
[33] A. Pesek, K. Hingerlt, F. Riesz, K. Lischka, Lattice misfit and relative tilt of lattice planes in semiconductor heterostructures, Semicond. Sci. Technol. 6 (1991) 705–708.
[34] R.J. Sichel, A. Grigoriev, D.-H. Do, S.-H. Baek, H.-W. Jang, C.M. Folkman, C.-B. Eom, Z. Cai, P.G. Evans, Anisotropic relaxation and crystallographic tilt in $BiFeO_3$ on miscut SrTiO3 (001), Appl. Phys. Lett. 96 (051901) (2010) 1–3.